IEEE Access
Multidisciplinary | Rapid Review | Open Access Journal

Received March 11, 2022, accepted March 25, 2022, date of publication April 6, 2022, date of current version April 12, 2022.

Digital Object Identifier 10.1109/ACCESS.2022.3165164

Analytical Calculation of Harmonics and Harmonic Losses in Five-Phase Carrier-Based PWM Voltage Source Inverters

PEGAH HAMEDANI[1], CRISTIAN GARCIA[2], (Member, IEEE), AND JOSE RODRIGUEZ[3], (Life Fellow, IEEE)

[1]Department of Railway Engineering and Transportation Planning, University of Isfahan, Isfahan 8174673441, Iran
[2]Department of Electrical Engineering, Universidad de Talca, Curico 3340000, Chile
[3]Department of Engineering Science, Universidad Andres Bello, Santiago 8370146, Chile

Corresponding author: Pegah Hamedani (p.hamedani@eng.ui.ac.ir)

This work was supported in part by the Agencia Nacional de Investigación y Desarrollo (ANID) through Fondecyt under Grant FB0008, Grant ACT192013, and Grant 1210208.

ABSTRACT The main purpose of this paper is to analyze a five-phase Voltage Source Inverter (VSI) that is operated with the Pulse Width Modulation (PWM) switching technique. Double Fourier integral (DFI) analysis has been used to extract the harmonics of the line-to-line voltages. Moreover, the harmonic current ripple has been calculated for an effective inductive five-phase load with a regular pentagon connection. Correspondingly, a new closed-form solution for calculating the harmonic losses in five-phase VSIs has been derived. In addition, a new equation for the weighted total harmonic distortion (WTHD) index has been extracted for five-phase VSIs. To validate the suggested analytical solutions (i.e., harmonic losses and WTHD equations), the results are compared with the DFI calculation method and the method of applying the fast Fourier transform (FFT) to a simulated waveform. The results show that the proposed analytical method has high accuracy and requires less mathematical effort, especially at high-frequency ratio values. Finally, the study includes simulation results and the implementation of an experimental setup.

INDEX TERMS Closed-form solution, five-phase inverter, Fourier transform, harmonic distortion, harmonic loss, PWM modulation.

I. INTRODUCTION

Over the past few decades, multi-phase motor drives (those with more than three phases) have been the subject of many studies owing to their specific advantages [1]–[9]. Multi-phase motor drives benefit from higher reliability, more power density, higher efficiency, lower torque ripple, and lower current ratings in the inverter arms [10], [11]. Furthermore, the utilization of multi-phase machines offers the capability of controlling more motors simultaneously with a single inverter [12]–[14]. Recently, with the development of semiconductor technology and digital processors, the industry has been trending toward multi-phase drives in medium- and high-power applications such as aircrafts, ships, traction applications, and electric vehicles.

The associate editor coordinating the review of this manuscript and approving it for publication was Qiuye Sun.

In the literature, most studies in the area of multi-phase systems have investigated multi-phase motors [15], [16] and their controlling schemes [3]–[14].

In the field of modulation techniques of multi-phase VSIs, a variety of studies have been reported in recent decades [4]–[6], [17]–[21]. However, some areas still require further investigation.

The most well-known modulation techniques for multi-phase VSIs are the carrier-based PWM, the space vector modulation (SVM), and the selective harmonic elimination (SHE) techniques. The PWM method in multi-phase VSIs is an extension of the famous PWM strategy for three-phase VSIs. The PWM technique is less complicated than other switching methods and is independent of the phase numbers. These advantages become more significant in applications with a large number of phases, where other methods are more complex [21], [22].

Another phenomenon that has been witnesses in recent decades is the increased utilization of nonlinear loads such as power electronic converters which produce harmonics [23]. Harmonics have several disadvantages including equipment failure and malfunction, increasing core losses in machines and transformers, overheating and noise in machines and transformers, and vibration in machines. Moreover, harmonics might result in unexpected resonances and power system instability. Therefore, harmonic stability and resonance analysis have been widely researched. For stabilization studies, the line impedance cooperative stability region identification method has been proposed for grid-tied inverters under weak grids [24]. Another important issue caused by harmonics is the increased switching losses in power converters, which reduces their energy efficiency [25].

Due to the issues discussed above, the precise calculation of the harmonic components and determination of the harmonic losses are two significant issues in multiphase VSIs [25]–[27]. These issues become even more important in PWM-controlled VSIs used in high-power applications. However, the harmonic evaluation of a PWM waveform and determining the harmonic components is a complex issue [27]. A simple and general method is to apply the FFT to a computer simulated signal. Although this method requires fewer mathematical manipulations, the precision of the results is highly affected by the simulation's numerical round-off errors and detrimental effects arising from spectral leakage and picket fence effect phenomena. Moreover, this method requires high computing capacity. In contrast, analytical methods guarantee high precision extraction of harmonic components of the voltage signals in a PWM-controlled VSI [26], [27]. DFI analysis is a well-known analytical solution for extracting the harmonics of PWM signals [25], [27].

Nevertheless, the harmonic losses of the load, which originate from the load current harmonic components, are an important part of the load losses. Therefore, extracting a closed-form equation to calculate the harmonic losses is of great interest in high-power industrial applications. In [25], the harmonic components of a three-phase VSI with carrier-based PWM have been extracted based on DFI analysis, and accordingly, the harmonic losses have been calculated.

Therefore, the main goal of this paper is to provide a more accurate description of a five-phase VSI operated with the PWM switching technique. As a result, this work concentrates on the analytical calculation of harmonic components and harmonic losses in five-phase inverters. This investigation has been carried out using simulations and experiments.

The paper is organized as follows. Section II discusses the DFI analysis of the five-phase PWM inverter. A new closed-form equation for calculating the harmonic losses of a five-phase VSI is presented in Section III. Then in Section IV, the WTHD factor is analytically computed for the five-phase VSI and compared with that of the three-phase VSI. In Sections V and VI, the simulation and experimental results of the five-phase VSI are presented, respectively. The main contributions of this paper are that it:

- Presents the harmonic solution for the line-to-line voltages of a five-phase VSI.
- Provides a new closed-form equation for calculating the harmonic losses in a five-phase VSI with an effective inductive load.
- Develops a new closed-form equation for calculating the WTHD of a five-phase VSI.

II. DFI ANALYSIS OF A FIVE-PHASE PWM INVERTER

Fig. 1 shows a single-phase VSI that is controlled by comparing a sinusoidal reference and a triangular carrier.

The harmonic solution of the phase voltage $v_{an}(t)$ can be extracted using DFI analysis as follows [25]:

$$\begin{aligned} v_{an}(t) &= V_{dc} + MV_{dc}\cos(\omega_o t + \theta_o) \\ &+ \frac{4V_{dc}}{\pi}\sum_{m=1}^{\infty}\frac{1}{m}J_0\left(\frac{m\pi}{2}M\right)\sin\left(\frac{m\pi}{2}\right)\cos(m(\omega_c t+\theta_c)) \\ &+ \frac{4V_{dc}}{\pi}\sum_{m=1}^{\infty}\sum_{\substack{n=-\infty \\ (n\neq 0)}}^{\infty}\left[\begin{array}{l}\frac{1}{m}J_n\left(\frac{m\pi}{2}M\right)\sin((m+n)\frac{\pi}{2}) \\ \cos(m(\omega_c t+\theta_c)+n(\omega_o t+\theta_o))\end{array}\right] \end{aligned} \tag{1}$$

where ω_o and ω_c are the fundamental angular frequency and carrier angular frequency, respectively. Note that $m_f = \omega_c/\omega_o$ is the frequency modulation index and M is the amplitude modulation index. θ_o and θ_c are the initial phases of the fundamental and carrier waveform, respectively. m and n correspond to the carrier harmonics and the sideband harmonics, respectively. In addition, J_n is the n-th order Bessel Function of the first kind.

Fig. 2 represents the configuration of a five-phase PWM inverter. To generate the switching pulses of the inverter, the PWM technique with five sinusoidal modulating references and a triangular carrier has been applied, as shown in Fig 3-(a).

In Fig. 3-(b)-(c), the inverter phase voltages (v_{an} and v_{cn}) and the line-to-line output voltage (v_{an}) are depicted (p.u. of V_{dc}), respectively.

The vector diagram of the five-phase VSI is shown in Fig. 4-(a). It is clear that in a five-phase VSI, the maximum line-to-line voltages that can be generated are $v_{ac}(t)$, $v_{bd}(t)$, $v_{ce}(t)$, $v_{da}(t)$, and $v_{eb}(t)$. It can be proved that $\left|\overrightarrow{v_{ac}}\right| = 2\sin(2\pi/5)\left|\overrightarrow{v_{az}}\right| \approx 1.902\left|\overrightarrow{v_{az}}\right|$. Consequently, to achieve maximum line-to-line voltages in a five-phase VSI, the load should be connected like a regular pentagon with an appropriate configuration, as shown in Fig. 4-(b).

In the following paragraphs, the analytical solution of VSI phase voltages will be developed. Then, using the Fourier series of phase voltages, the harmonic spectrum of the line-to-line voltages will be derived.

By considering $\theta_c = 0$ in (1) and applying a phase shift of $2\pi/5$ to the reference signal, the phase voltages

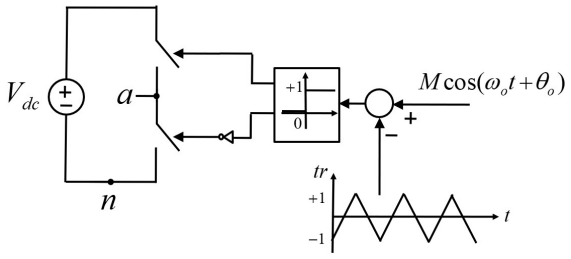

FIGURE 1. A single-phase VSI with PWM switching technique.

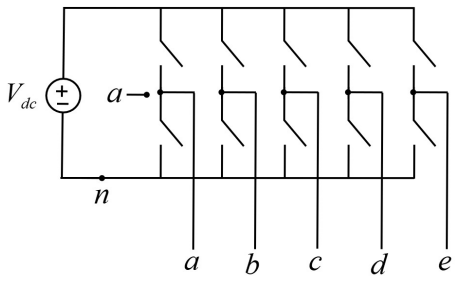

FIGURE 2. Configuration of the five-phase VSI.

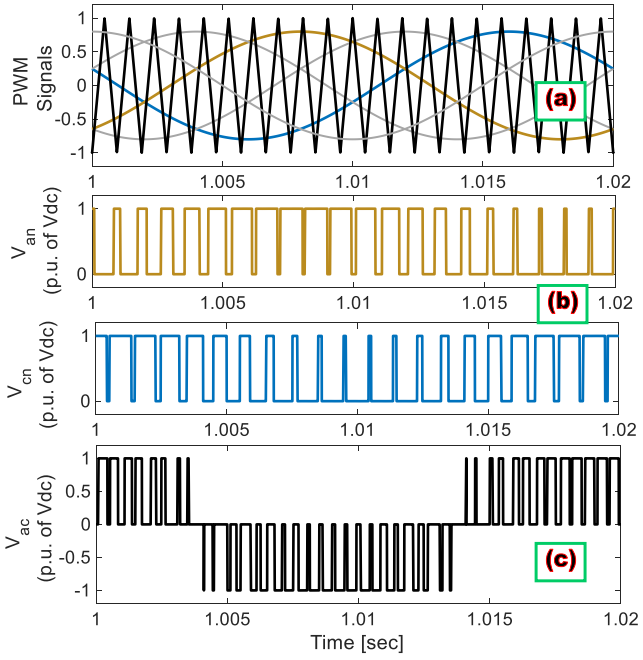

FIGURE 3. (a) Sinusoidal references and triangular carrier of PWM technique, (b) inverter phase voltages (v_{an} and v_{cn}), (c) inverter line-to-line voltage (v_{ac}).

$v_{an}(t)\ldots, v_{en}(t)$ can be expressed as follows:

$$v_{an}(t) = V_{dc} + MV_{dc}\cos(\omega_o t) + \frac{4V_{dc}}{\pi}\sum_{m=1}^{\infty}\sum_{n=-\infty}^{\infty}\left[\frac{1}{m}J_n(\frac{m\pi}{2}M)\sin((m+n)\frac{\pi}{2}) \cos(m\omega_c t + n\omega_o t)\right] \quad (2)$$

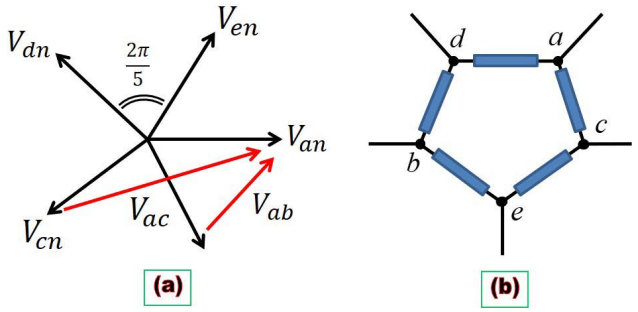

FIGURE 4. (a) Vector diagram of the five-phase VSI, (b) The five-phase load with regular pentagon connection.

$$v_{bn}(t) = V_{dc} + MV_{dc}\cos(\omega_o t - \frac{2\pi}{5}) + \frac{4V_{dc}}{\pi}\sum_{m=1}^{\infty}\sum_{n=-\infty}^{\infty}\left[\frac{1}{m}J_n(\frac{m\pi}{2}M)\sin((m+n)\frac{\pi}{2}) \cos(m\omega_c t + n\omega_o t - \frac{2\pi}{5})\right] \quad (3)$$

$$\vdots$$

$$v_{en}(t) = V_{dc} + MV_{dc}\cos(\omega_o t - \frac{8\pi}{5}) + \frac{4V_{dc}}{\pi}\sum_{m=1}^{\infty}\sum_{n=-\infty}^{\infty}\left[\frac{1}{m}J_n(\frac{m\pi}{2}M)\sin((m+n)\frac{\pi}{2}) \cos(m\omega_c t + n\omega_o t - \frac{8\pi}{5})\right] \quad (4)$$

As mentioned above, with respect to the vector diagram shown in Fig. 4-(a), the line-to-line voltages ($v_{ac}(t)$, $v_{bd}(t)$, $v_{ce}(t)$, $v_{da}(t)$, and $v_{eb}(t)$) are considered and calculated in this work. By considering (2)-(4) and using trigonometric relations, the line-to-line voltages will be computed. Details of these calculations are given in the Appendix. The maximum line-to-line voltages can be expressed as:

$$v_{ac}(t) = 2\sin\frac{2\pi}{5}MV_{dc}\cos(\omega_o t + \frac{\pi}{10}) + \frac{8V_{dc}}{\pi}\sum_{m=1}^{\infty}\sum_{n=-\infty}^{\infty}\left[\frac{1}{m}J_n(\frac{m\pi}{2}M)\sin((m+n)\frac{\pi}{2}) \sin(\frac{2n\pi}{5})\cos(m\omega_c t + n(\omega_o t - \frac{2\pi}{5}) + \frac{\pi}{2})\right] \quad (5)$$

$$v_{bd}(t) = 2\sin\frac{2\pi}{5}MV_{dc}\cos(\omega_o t - \frac{3\pi}{10}) + \frac{8V_{dc}}{\pi}\sum_{m=1}^{\infty}\sum_{n=-\infty}^{\infty}\left[\frac{1}{m}J_n(\frac{m\pi}{2}M)\sin((m+n)\frac{\pi}{2}) \sin(\frac{2n\pi}{5})\cos(m\omega_c t + n(\omega_o t - \frac{4\pi}{5}) + \frac{\pi}{2})\right] \quad (6)$$

$$\vdots$$

$$v_{eb}(t) = 2\sin\frac{2\pi}{5}MV_{dc}\cos(\omega_o t - \frac{3\pi}{2}) + \frac{8V_{dc}}{\pi}\sum_{m=1}^{\infty}\sum_{n=-\infty}^{\infty}\left[\begin{array}{l}\frac{1}{m}J_n(\frac{m\pi}{2}M)\sin((m+n)\frac{\pi}{2}) \\ \sin(\frac{3n\pi}{5})\cos(m\omega_c t \\ \quad + n(\omega_o t - \pi) - \frac{\pi}{2})\end{array}\right] \tag{7}$$

The maximum line-to-line voltages for three-phase and seven-phase VSIs can be calculated in the same way. The results are represented in Table 1 of the Appendix.

In Fig. 5, the dominant harmonic components of the line-to-line voltage v_{ac} are given as a function of M in the five-phase VSI.

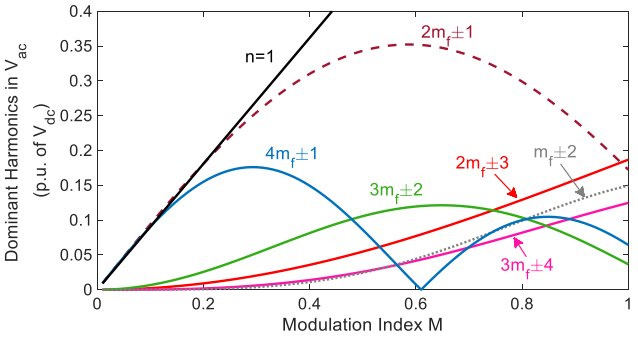

FIGURE 5. Dominant harmonics of line-to-line voltage v_{ac} in the five-phase PWM inverter according to M.

Figs. 6 and 7 show the v_{ac} line-to-line voltage frequency spectrum relative to the fundamental in the five-phase VSI using the analytical and simulation methods for $M = 0.8$ with $m_f = 15, 17$, respectively.

It is clear that the harmonic amplitudes in the line-to-line voltage spectrums achieved from the analytical and simulation methods are relatively close. However, the simulation method takes more time, and the precision of its results is highly affected by numerical round-off errors and detrimental effects arising from spectral leakage and the picket fence effect.

III. LOSSES CALCULATION

To determine a closed-form formula for calculating the harmonic losses in five-phase VSIs, correct and logical assumptions must first be made. Therefore, some indispensable simulation results, which help evaluate the waveform variations more precisely and make reasonable assumptions, are initially provided.

In Fig. 8, the line-to-line voltage (v_{ac}), its fundamental component, and the corresponding harmonic current ripple, Δi_{ac}, are represented for $m_f = 21$, $M = 0.8$ with an effective inductive load. It can be seen that the load current has a high-frequency ripple that is twice the switching frequency ($2f_c$).

In Fig. 9-(a)-(b), the inverter phase voltages (v_{an} and v_{cn}) and the triangular carrier are represented in an arbitrary switching period, $\Delta T = 1/f_c$. In Fig. 9-(c), the inverter line-to-line voltage (v_{ac}), the harmonic current ripple (Δi_{ac}), and the average load EMF (e_{ac}) are shown in an arbitrary switching period. It is evident that the average load EMF, e_{ac}, can be assumed to be constant during the switching period ΔT. Moreover, for an effective inductive load, the current ripple, Δi_{ac}, has linear variations.

In Fig. 10, the current ripple (Δi_{ac}) and the five-phase line-to-line voltages ($v_{ac}(t)$, $v_{bd}(t), \ldots, v_{eb}(t)$) are depicted in an arbitrary switching period ΔT. It is clear from the figures that every line-to-line voltage waveform has two active pulses in each switching period ΔT, and that each of the pulses occurs in half of the cycle of the switching period ΔT. However, as shown in Fig. 10, the active pulses are not necessarily located in the middle of the half cycles $\Delta T/2$.

Based on the above discussion, in Fig. 11, an expanded sketch of Fig. 8 over an arbitrary switching interval ΔT is represented using the following assumptions:

1) The average load EMF, e_{ac}, is assumed to be constant during the switching period $\Delta T = 1/f_c$.

2) The ohmic loss of the fundamental current component, which does not affect the harmonic losses, is not considered in the upcoming discussion.

3) It is supposed that the five-phase load is effective inductive, which leads to linear variations of the current ripple, Δi_{ac}.

4) The active pulses in the output line-to-line voltages are not located in the middle of the half cycles $\Delta T/2$.

According to Fig. 11, the current ripple Δi_{ac}, which is the difference between the actual current and the fundamental component, can be calculated for all the periods T_1, T_2, and T_3 as follows:

For $0 \le t \le T_1$:

$$\Delta i_{ac}(t) = -\frac{e_{ac}}{L_\sigma}t = \frac{V_{dc}}{L_\sigma}(u_1 - u_2)t \tag{8}$$

For $T_1 \le t \le T_2$:

$$\Delta i_{ac}(t) = \frac{V_{dc}}{L_\sigma}[2 - (u_1 - u_2)](t - T_1) - \frac{V_{dc}}{L_\sigma}(u_1 - u_2)t \tag{9}$$

For $T_1 + T_2 \le t \le T_1 + T_2 + T_3$:

$$\Delta i_{ac}(t) = -\frac{V_{dc}}{L_\sigma}[(u_1 - u_2)(t - T_1 - T_2)] + \frac{V_{dc}}{L_\sigma}[2 - (u_1 - u_2)]T_2 - \frac{V_{dc}}{L_\sigma}(u_1 - u_2)T_1 \tag{10}$$

where L_σ is the load inductance and $u_1 - u_2 = e_{ac}/V_{dc}$, with $u_1 = e_{an}/V_{dc}$ and $u_2 = e_{dn}/V_{dc}$.

Furthermore, it can be proved that:

$$T_1 = (1 - u_1)\frac{\Delta T}{4} \tag{11}$$

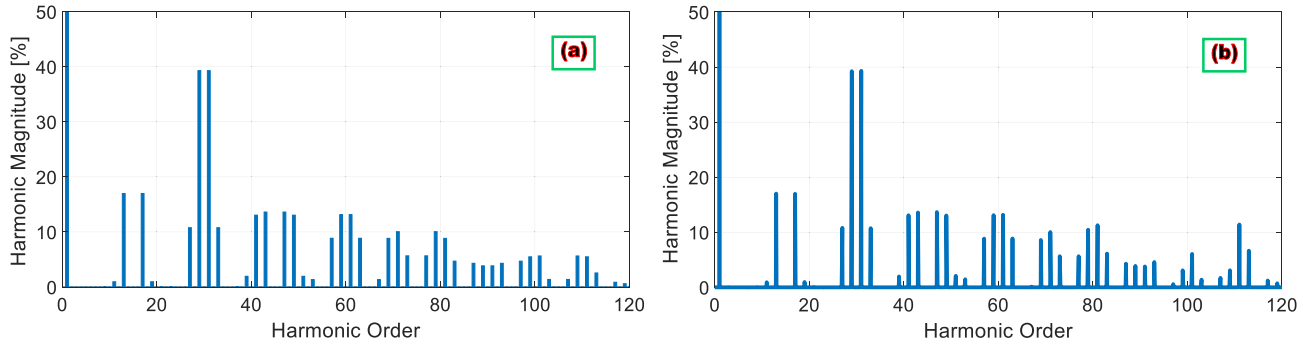

FIGURE 6. Harmonic spectrum of line-to-line voltage v_{ac} in the five-phase inverter for $M = 0.8$ and $m_f = 15$: (a) analytical method, (b) simulation method.

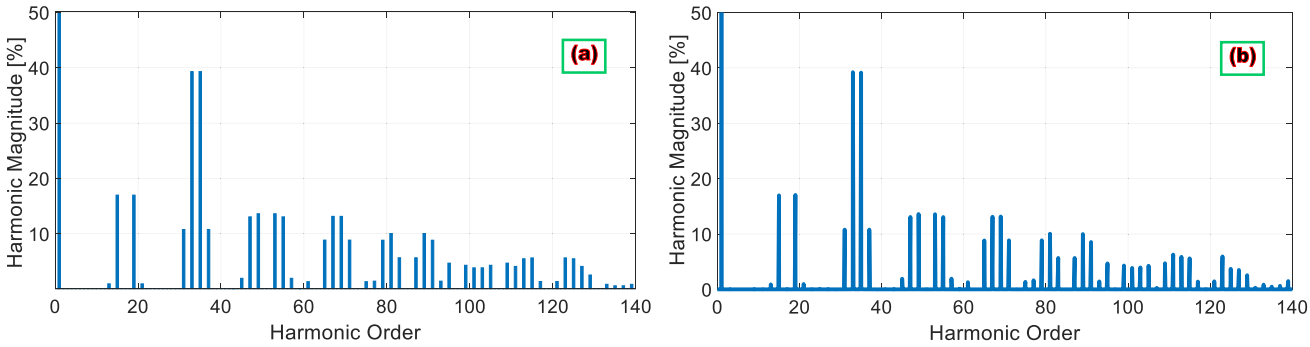

FIGURE 7. Harmonic spectrum of line-to-line voltage v_{ac} in the five-phase inverter for $M = 0.8$ and $m_f = 17$: (a) analytical method, (b) simulation method.

$$T_2 = (u_1 - u_2)\frac{\Delta T}{4} \tag{12}$$

$$T_3 = (1 + u_2)\frac{\Delta T}{4} \tag{13}$$

The average squared current ripple $\left\langle \Delta i_{ac}^2(t) \right\rangle$ can be defined as follows:

$$\left\langle \Delta i_{ac}^2(t) \right\rangle = \frac{2}{\Delta T} \int_0^{\frac{\Delta T}{2}} \Delta i_{ac}^2(t) dt \tag{14}$$

Substituting (8)-(10) into (14) and simplifying gives:

$$\left\langle \Delta i_{ac}^2(t) \right\rangle = \left(\frac{V_{dc}}{L_\sigma}\right)^2 \frac{\Delta T^2}{48} \begin{bmatrix} (u_2 - u_1)^2 + (u_2 - u_1)^3 \\ + (u_2 - u_1)(u_2^3 - u_1^3) \end{bmatrix} \tag{15}$$

On the other hand, from the modulation strategy of the five-phase inverter, it can be shown that:

$$u_1 = \frac{e_a}{V_{dc}} \approx \frac{(v_{an})_1}{V_{dc}} = M \cos\theta \tag{16}$$

$$u_2 = \frac{e_c}{V_{dc}} \approx \frac{(v_{cn})_1}{V_{dc}} = M \cos(\theta - \frac{4\pi}{5}) \tag{17}$$

Substituting (16)-(17) into (15) and manipulating the equation, results in:

$$\left\langle \Delta i_{ac}^2(t) \right\rangle = \left(\frac{V_{dc}}{L_\sigma}\right)^2 \frac{\Delta T^2}{48} \begin{bmatrix} 4M^2 \sin^2\frac{2\pi}{5} \cos^2(\theta + \frac{\pi}{10}) \\ -8M^3 \sin^3\frac{2\pi}{5} \cos^3(\theta + \frac{\pi}{10}) \\ -2M^4 \sin\frac{2\pi}{5} \cos(\theta + \frac{\pi}{10}) \\ \left(\cos^3(\theta - \frac{4\pi}{5}) - \cos^3\theta\right) \end{bmatrix} \tag{18}$$

The harmonic current ripple can be defined as:

$$I_h = \sqrt{\left(\frac{1}{T}\int_0^T \Delta i_{ac}^2(t) dt\right)} \equiv \sqrt{\left\langle \Delta i_{ac}^2(t) \right\rangle} \tag{19}$$

Accordingly, the harmonic losses can be written as:

$$P_{h,cu} = R_e i_{h,ave}^2 = R_e . \frac{1}{T}\int_T I_h^2 d\theta \tag{20}$$

where R_e is the load resistance. It should be noted that the above integration is only valid for $e_{ac} \geq 0$, which leads to:

$$\begin{aligned} e_{ac} &\approx (v_{ac})_1 = 2\sin 5MV_{dc}\cos(\omega_0 t + \frac{\pi}{10}) \\ &= 2\sin\frac{2\pi}{5} MV_{dc}\cos(\theta + \frac{\pi}{10}) \geq 0 \end{aligned} \tag{21}$$

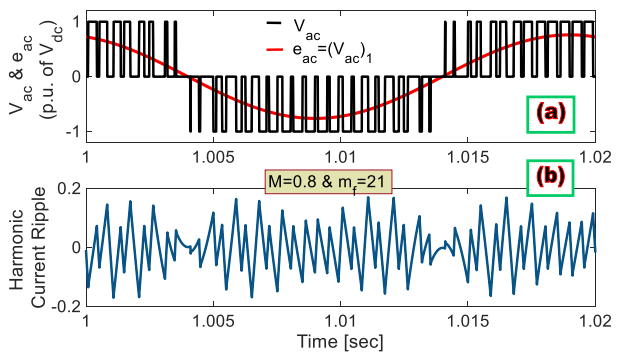

FIGURE 8. (a) Inverter line-to-line voltage (v_{ac}) and its fundamental component (e_{ac}), (b) harmonic current ripple of the five-phase VSI.

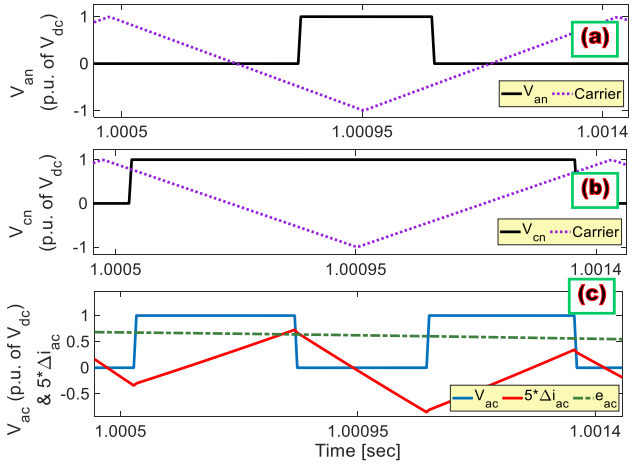

FIGURE 9. (a) Inverter phase voltages (v_{an}) and triangular carrier, (b) inverter phase voltages (v_{dn}) and triangular carrier, (c) inverter line-to-line voltage (v_{ac}), harmonic current ripple (Δi_{ac}), and the average load EMF (e_{ac}) in an arbitrary switching period.

The valid integration interval is thus given by:

$$-\frac{\pi}{2} \le \theta + \frac{\pi}{10} \le \frac{\pi}{2} \Rightarrow -\frac{3\pi}{5} \le \theta \le \frac{2\pi}{5} \tag{22}$$

Using (22), the average squared harmonic current ripple can be written as:

$$I_{h,ave}^2 = \frac{1}{\pi} \int_{-\frac{3\pi}{5}}^{\frac{2\pi}{5}} I_h^2 d\theta = \frac{1}{\pi} \int_{-\frac{3\pi}{5}}^{\frac{2\pi}{5}} \left\langle i_{ac}^2 \right\rangle d\theta \tag{23}$$

Substituting (18) into (23) and simplifying gives:

$$I_{h,ave}^2 = \left(\frac{V_{dc}}{L_\sigma}\right)^2 \frac{\Delta T^2}{48} \begin{bmatrix} 2M^2 \sin^2 \frac{2\pi}{5} \\ -\frac{32}{3\pi} M^3 \sin^3 \frac{2\pi}{5} \\ +\frac{3}{2} M^4 \sin^2 \frac{2\pi}{5} \end{bmatrix} \tag{24}$$

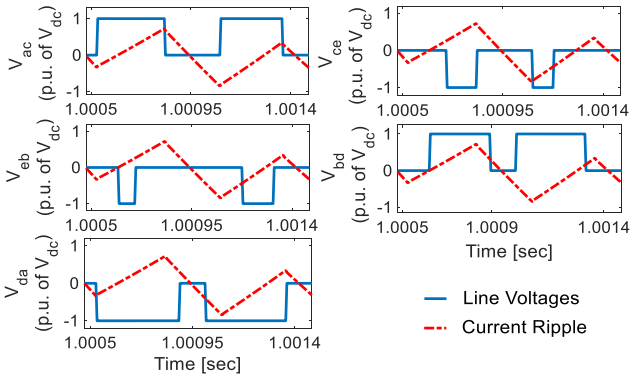

FIGURE 10. The five-phase VSI line-to-line voltages and the current ripple in an arbitrary switching period.

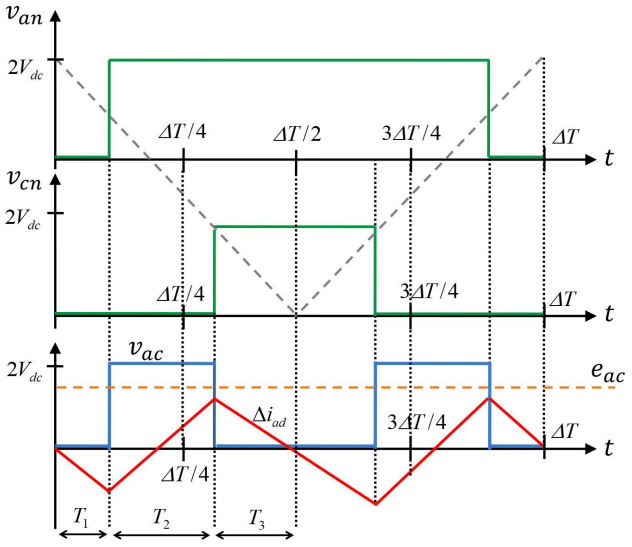

FIGURE 11. An expanded sketch of the switching interval in the PWM technique of the five-phase VSI.

Consequently, by substituting (24) into (20), the harmonic loss expression can be calculated as:

$$P_{h,cu} = R_e \cdot \left(\frac{V_{dc}}{L_\sigma}\right)^2 \frac{\Delta T^2}{48} f(M) \tag{25}$$

where $f(M) = 2M^2 \sin^2 \frac{2\pi}{5} - \frac{32}{3\pi} M^3 \sin^3 \frac{2\pi}{5} + \frac{3}{2} M^4 \sin^2 \frac{2\pi}{5}$.

Note that for a three-phase VSI, $f(M)$ can be written as [25]:

$$f(M) = \frac{3}{2} M^2 - \frac{4\sqrt{3}}{\pi} M^3 + \frac{9}{8} M^4 \tag{26}$$

Fig. 12 represents $f(M)$ as a function of M for the five- and three-phase VSI. It is clear that for higher M values, the harmonic loss in the five-phase VSI is lower than the three-phase VSI. The harmonic loss for three-phase and seven-phase VSIs can be expressed in the same way. The results are given in Table 1 in the Appendix.

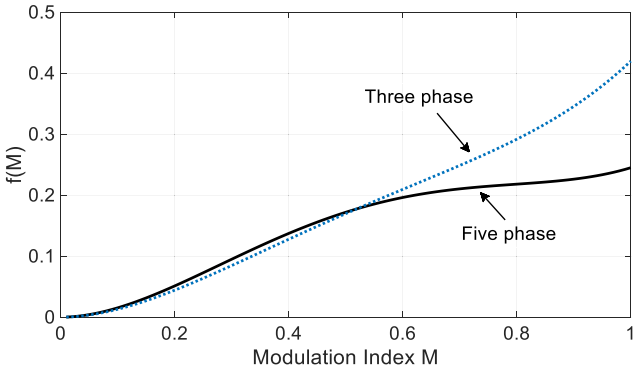

FIGURE 12. Function $f(M)$ according to M in the five-phase and three-phase VSIs.

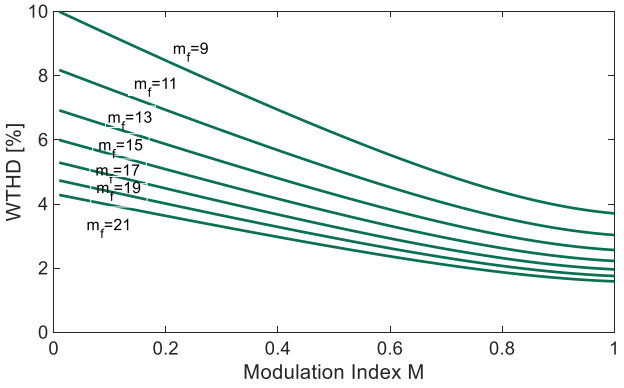

FIGURE 13. WTHD according to M for different values of m_f in the five-phase VSI.

IV. WTHD CALCULATION

For a voltage signal, the WTHD0 and WTHD can be defined as:

$$WTHD0 = \frac{\sqrt{\sum_{n=2}^{\infty} \frac{V_n^2}{n^2}}}{V_1\,|_{M=1}} = \frac{\sqrt{\sum_{n=2}^{\infty} \frac{V_n^2}{n^2}}}{2\sin\frac{2\pi}{5}V_{dc}} \tag{27}$$

$$WTHD = \frac{\sqrt{\sum_{n=2}^{\infty} \frac{V_n^2}{n^2}}}{V_1} = \frac{WTHD0}{M} \tag{28}$$

where V_n is the magnitude of the n-th harmonic in the line-to-line voltage and V_1 is the fundamental component magnitude of the line-to-line voltage at $M = 1$ and is equal to $2\sin(2\pi/5)V_{dc} \approx 1.902V_{dc}$.

The magnitude of the current harmonics can be determined from the line-to-line voltage harmonics as follows:

$$I_n = \frac{V_n}{\omega_n L_\sigma} = \frac{V_n}{n}\frac{1}{\omega_o L_\sigma} \tag{29}$$

Accordingly, the Root-Mean-Square (RMS) value of the harmonic current can be written as:

$$I_{h,ave}^2 = \sum_{n=2}^{\infty} \frac{1}{2} I_n^2 \tag{30}$$

Substituting (29) into (30) gives:

$$I_{h,ave}^2 = \sum_{n=2}^{\infty} \frac{1}{2}\left(\frac{V_n}{n}\frac{1}{\omega_o L_\sigma}\right)^2 \tag{31}$$

Or alternatively:

$$\sum_{n=2}^{\infty} \frac{V_n^2}{n^2} = 2\omega_o^2 L_\sigma^2 I_{h,ave}^2 \tag{32}$$

Substituting (32) into (27) leads to:

$$WTHD0 = \frac{\sqrt{2}\omega_o L_\sigma I_{h,ave}}{2\sin\frac{2\pi}{5}V_{dc}} \tag{33}$$

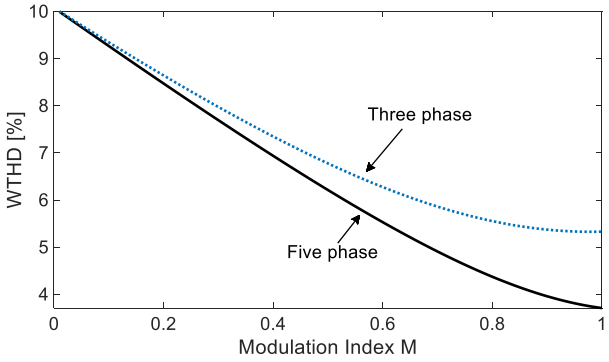

FIGURE 14. WTHD in the three- and five-phase VSI for $m_f = 9$.

Further substituting (24) into (33) and simplifying, considering $\Delta T = 1/f_c$ and $\omega_o = 2\pi f_o$, gives:

$$WTHD0 = \frac{\pi\sqrt{f(M)}}{\sqrt{24}\sin\frac{2\pi}{5}f_c/f_o} \tag{34}$$

where f_c/f_o is the frequency modulation index m_f.

In Fig. 13, the WTHD is plotted according to M for different values of m_f ($m_f = 9, 11, 13, 15, 17, 19, 21$). As expected, the WTHD decreases as the m_f value increases.

Furthermore, the WTHD in five-phase and three-phase VSIs with respect to M is represented for $m_f = 15$ in Fig. 14. It is clear that the WTHD of the five-phase VSI is smaller than that of its three-phase counterpart, and this difference increases at higher M values.

V. SIMULATION RESULTS

To confirm the accuracy of the derived equations, several tests have been performed under various operating conditions. The simulation of the complete five-phase VSI has been performed using PSCAD/EMTDC software. The five-phase VSI supplies a resistive-inductive load with a regular pentagon connection, according to Fig. 4-(b).

The simulation parameters are compatible with the experimental setup discussed in the next section. The load has a resistance of 10 Ω and an inductance of 20 mH in each phase.

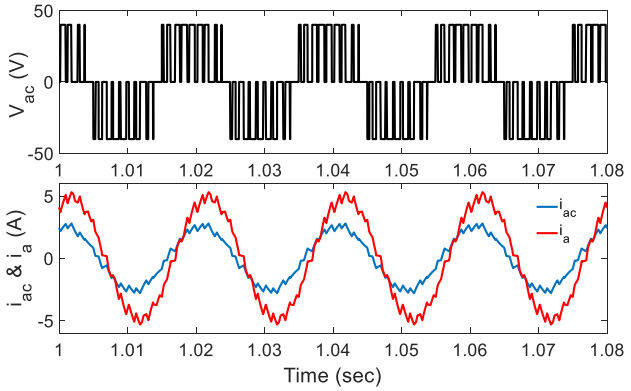

FIGURE 15. The line-to-line voltage v_{ac}, the line current i_a, and the phase current i_{ac} of the five-phase VSI.

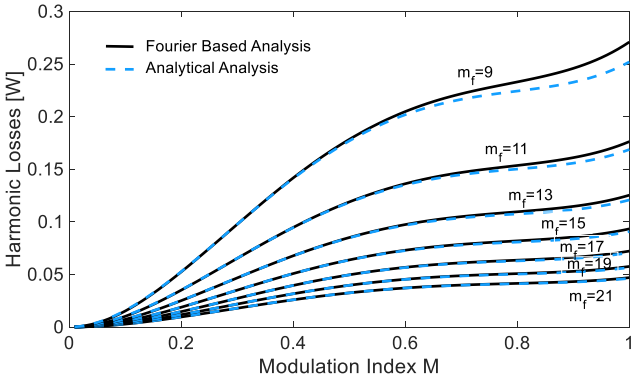

FIGURE 16. Harmonic losses of the five-phase VSI according to M for different values of m_f.

The dc-link voltage is equal to 40 V. Some of the simulation results are presented below.

In Fig. 15, the line-to-line voltage v_{ac}, the line current i_a, and the phase current i_{as} of the five-phase PWM inverter are illustrated for $M = 0.8$ and $m_f = 9$. It is evident that the ratio of the line current magnitude to the phase current magnitude is equal to $2\sin(2\pi/5) \approx 1.902$.

In Fig. 16, the harmonic losses of the five-phase VSI have been extracted and represented using the analytical method and the DFI analysis method. The harmonic losses are depicted along with the amplitude modulation index M for different values of m_f ($m_f = 9, 11, 13, 15, 17, 19, 21$).

In the analytical method, the harmonic losses are calculated using the closed-form equation (25) derived from the harmonic current ripple. In the DFI analysis approach, the voltage harmonic components are first extracted using (5)-(7). Then, to compute the current harmonic components, each voltage component is divided by its corresponding impedance value. Subsequently, the RMS values of the current harmonic components can be extracted. Finally, the harmonic losses are calculated from the summation of the ohmic losses of all harmonic components.

The results from the analytical method are clearly in accordance with those of the DFI-based analysis method, which proves the precision of the former. However, at lower m_f values, the accuracy of the analytical method will decrease because its required assumptions are not fully met.

To achieve a more complete evaluation, the normalized value of the harmonic losses with respect to the current loss of the fundamental component should be considered. Fig. 17 demonstrates the normalized harmonic losses of the five-phase VSI according to M for different values of m_f ($m_f = 9, 11, 13, 15, 17, 19, 21$) for both the analytical and the double Fourier integral based analysis methods.

In Fig. 18, the harmonic losses and normalized harmonic losses of the five-phase VSI (with $m_f = 9$) have been represented and compared using three different methods:

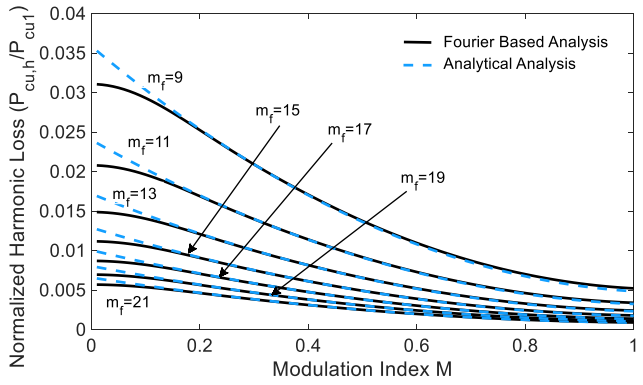

FIGURE 17. Normalized harmonic losses of the five-phase VSI according to M for different values of m_f.

- Analytical method (closed-form equation)
- DFI analysis method
- The method of applying the FFT to a simulated waveform

In the method of applying the FFT to a simulated waveform, the first step is to generate the harmonic current waveform of the VSI using PSCAD/EMTDC software. Then, the harmonic components of the simulated current waveform are extracted by applying the FFT with the frequency resolution of 5 Hz. Subsequently, the harmonic losses are calculated from the summation of the ohmic losses of all harmonic components. This process should be repeated for different m_f and M values. Therefore, the outcome is a set of distinct values and is thus discontinuous.

In order to make a more valuable comparison, the error and the calculation times of each of the three methods are provided in Tables 2-4 in the Appendix. For example, for $m_f = 9$ and a fixed set of M values, the average error of the harmonic loss calculation in the analytical method is 2.85%. Therefore, as compared to the simulation method, which has an error of 6.42%, the analytical method provides greater accuracy in calculating the harmonic loss. Moreover, using the analytical method for the same set of M values, the average error of the harmonic loss calculation for

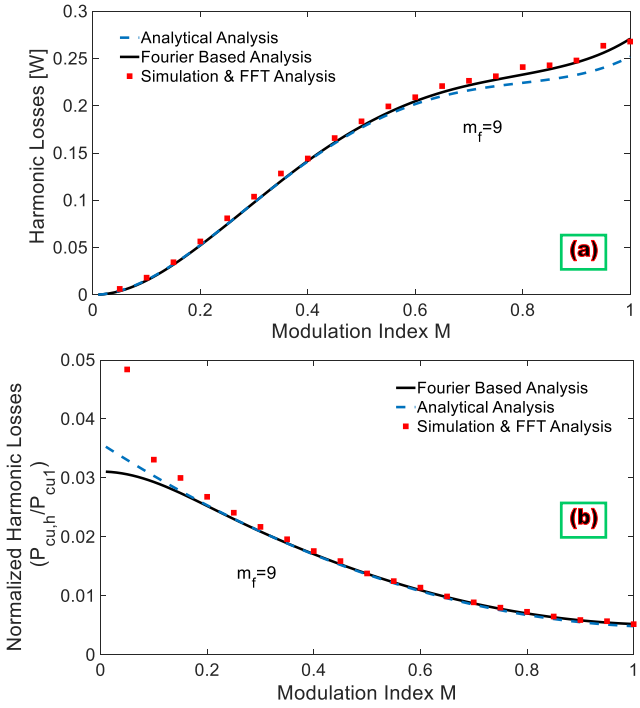

FIGURE 18. (a) Harmonic losses, and (b) normalized harmonic losses of the five-phase VSI according to M for $m_f = 9$ using three different methods.

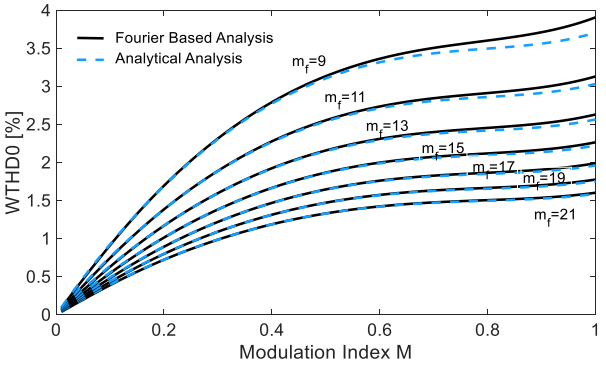

FIGURE 19. WTHD0 of the five-phase VSI according to M for different values of m_f.

$m_f = 21$ is 1.09%, which demonstrates that the accuracy increases in higher frequency ratio values. Unlike the DFI analysis method and the simulation and FFT method, the proposed closed-form equation for harmonic losses requires no simulation or program writing, and it has considerably fewer mathematical operations.

Fig. 19 shows the WTHD0 results of the five-phase VSI in terms of the amplitude modulation index M for different values of m_f ($m_f = 9, 11, 13, 15, 17, 19, 21$) using both the analytical method and the DFI analysis method. It is evident that the results from the analytical method are in accordance with the double Fourier integral analysis method. This proves the precision of the analytical method, especially at high m_f values.

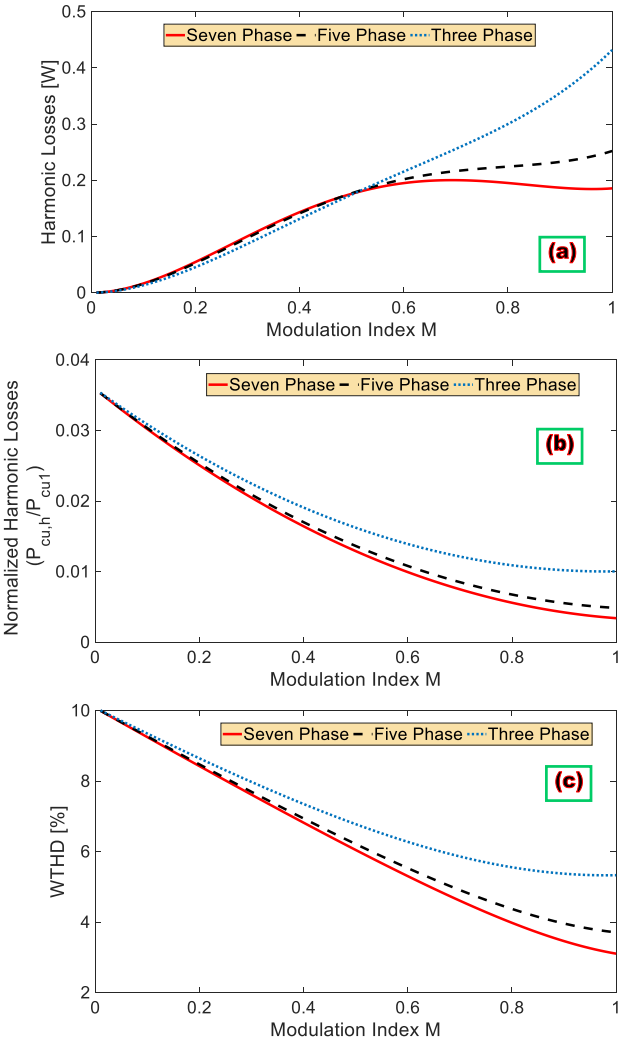

FIGURE 20. Comparison of the seven-phase, five-phase, and three-phase VSIs for $m_f = 9$: (a) Harmonic losses, (b) Normalized harmonic losses, (c) WTHD.

In Fig. 20, the harmonic losses, normalized harmonic losses, and current WTHD of the seven-phase, five-phase, and three-phase VSIs are represented with respect to M for $m_f = 9$.

As can be seen in the figures, by increasing the phase numbers, the harmonic losses and WTHD decrease, and the difference becomes more significant in high amplitude modulation index values.

VI. EXPERIMENTAL RESULTS

To verify the simulation results, a five-phase inverter setup has been built utilizing PM50CTJ060 600V/50A Mitsubishi IPMs. The five-phase VSI is supplied through a dc power supply. A Gate driver board has been designed to fire the IGBT switches. The 74HCT244N Buffer IC has been utilized for amplifying the current values, and TLP521 Photo-couplers have been used for isolating the power circuit and the DSP board. In addition, a protection circuit has been added to

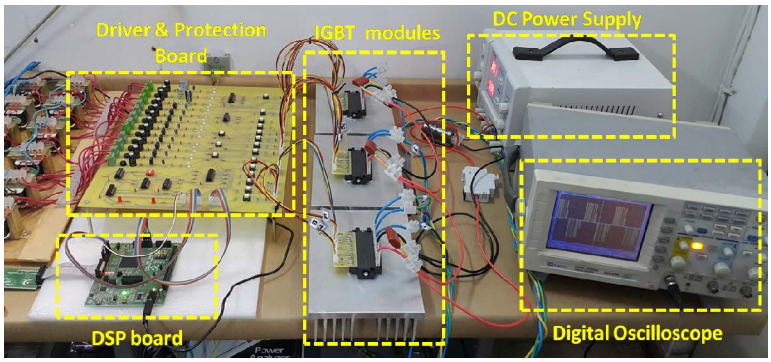

FIGURE 21. Photograph of the five-phase VSI experimental setup.

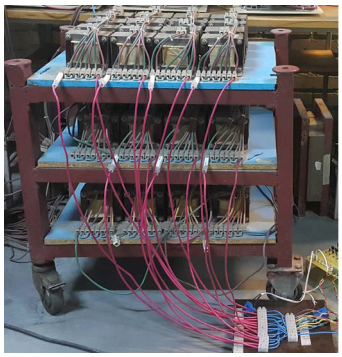

FIGURE 22. Photograph of the five-phase load.

the Gate driver board; it prevents simultaneous conduction of up and down switches by controlling the enable pin of the Buffer IC using 74ALS08 NAND and 74HC4078 OR ICs. The PWM switching technique is programmed with the Code Composed Studio (CCS). It is implemented utilizing a TMS320F2812 Digital Signal Processor (DSP) board and connected to a PC through an XDS100 Emulator to compile and load the programs. An Instek GDS-820 digital oscilloscope has been utilized to monitor the results. Furthermore, the current and voltage waveforms are measured using LA55/P and LV25P/SP2 LEM sensors, respectively. Moreover, the waveforms are sampled utilizing an Advantech portable data acquisition module, USB-4711A, with a sampling rate of 10 kHz.

Photographs of the implemented five-phase VSI experimental setup and the five-phase resistive-inductive load with a regular pentagon connection are shown in Figs. 21 and 22, respectively. The hardware setup parameters are as follows: the five-phase resistive-inductive load has $R = 10\ \Omega$ and $L = 20$ mH in each phase. The voltage of the dc power supply is equal to 40 V. The fundamental frequency is considered $f_1 = 50$ Hz. The pulses are generated with an accuracy of 200 μs.

To compare the experimental and simulation results, Fig. 23 depicts the line current i_a, phase current i_{ac}, and the line-to-line voltage v_{ac} of the five-phase VSI achieved by each set-up for $M = 0.8$ and $m_f = 7$.

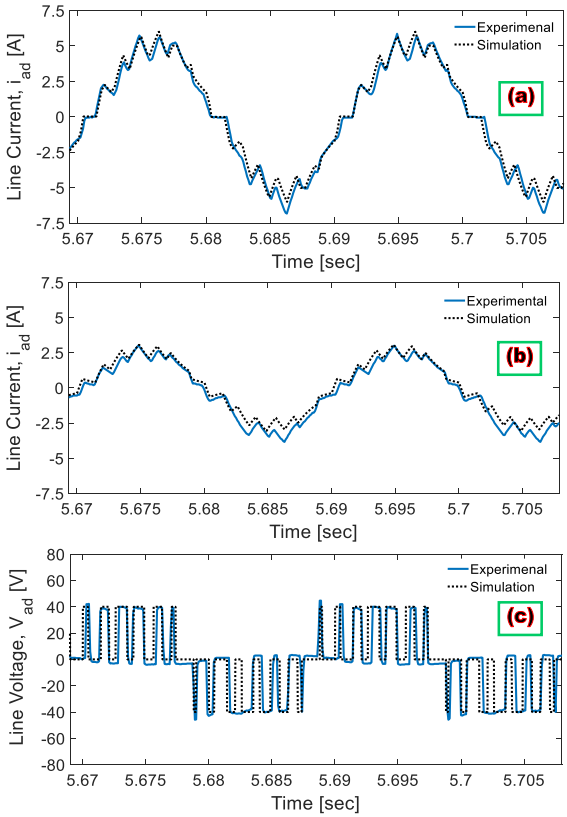

FIGURE 23. Experimental and simulation results of the five-phase VSI: (a) line current i_a, (b) phase current i_{ac}, c) line-to-line voltage v_{ac} with $M = 0.8$ and $m_f = 7$.

The experimental results are compatible with the simulation results, which validates the accuracy of the simulation results. The negligible differences between the two are due to the diodes' forward voltage drops and the small imbalance in the five-phase loads.

Fig. 24 shows the v_{ac} line-to-line voltage frequency spectrum with respect to the fundamental in the five-phase VSI using the analytical method, simulation method, and experimental results for $M = 0.8$ with $m_f = 7$. The simulation parameters, such as snubbers and the turn-on delay time

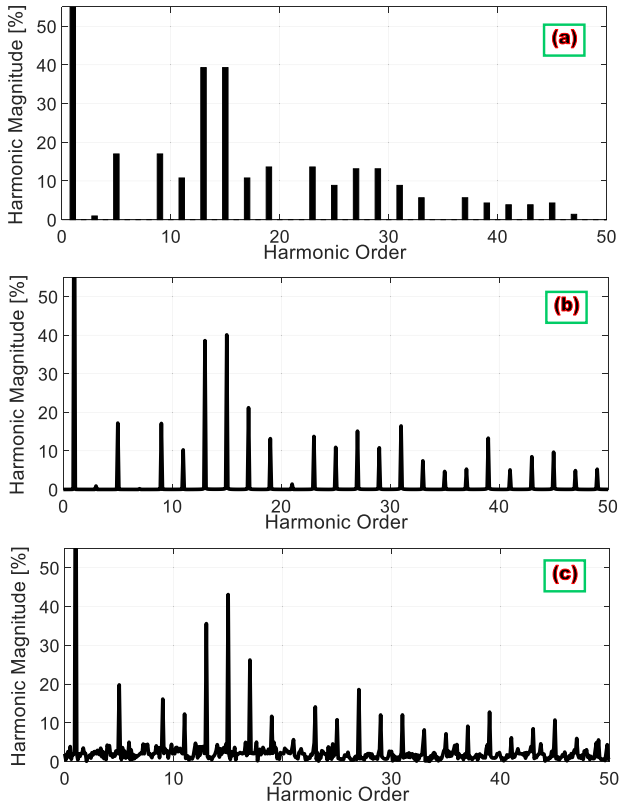

FIGURE 24. Harmonic spectrum of line-to-line voltage v_{ac} in the five-phase VSI for $M = 0.8$ and $m_f = 7$: (a) analytical method, (b) simulation method, (c) experimental result.

between up and down switches, match the experimental setup as closely as possible.

Note that the frequency spectrums shown in Figs. 24-(b)-(c) are extracted by applying the FFT to the simulated and experimental voltage waveforms shown in Fig. 23-(c), respectively.

The results show negligible differences in the magnitude of the harmonics in the frequency spectrums. However, the harmonic orders of the spectrum in the simulation and experimental results correlate closely with that of the analytical method.

VII. CONCLUSION

Due to the importance of power quality evaluation and the calculation of harmonic losses of multi-phase VSIs in high-power applications, this paper focuses on the analysis of harmonics and harmonic losses in five-phase VSIs with PWM switching schemes. In this paper, using the DFI analysis, the harmonic content of the line-to-line voltages in the five-phase PWM inverter has been extracted. Accordingly, new closed-form solutions for calculating harmonic losses and the WTHD index have been derived for the five-phase VSI with a regular pentagon load connection.

The results show that the harmonic loss in the five-phase VSI is lower than that of the three-phase VSI for high amplitude modulation index values. Also, the WTHD of the five-phase VSI is smaller than that of its three-phase counterparts, and this difference increases at higher amplitude modulation index values. Moreover, the extracted closed-form solutions require less calculation effort and are sufficiently accurate, especially at high-frequency ratio values. For $m_f = 9$ and a fixed set of M values, the average error of harmonic loss calculation in the analytical method is 2.85% whereas the simulation method has an error rate of 6.42%; the analytical method thus calculates the harmonic loss more accurately. In addition, for the same set of M values, the average error of harmonic loss calculation in the analytical method for $m_f = 21$ is 1.09%, which indicates that the accuracy increases in higher frequency ratio values. Unlike the DFI analysis method and the simulation and FFT method, the proposed closed-form equation for harmonic loss requires neither simulation nor program writing; it also involves considerably fewer mathematical operations.

APPENDIX

The phase voltages of the five-phase VSI can be written as:

$$v_{an}(t) = V_{dc} + MV_{dc}\cos(\omega_o t) + \frac{4V_{dc}}{\pi}\sum_{m=1}^{\infty}\sum_{n=-\infty}^{\infty}\left[\frac{1}{m}J_n(\frac{m\pi}{2}M)\sin((m+n)\frac{\pi}{2})\cos(m\omega_c t + n\omega_o t)\right] \quad (A.1)$$

$$v_{bn}(t) = V_{dc} + MV_{dc}\cos(\omega_o t - \frac{2\pi}{5}) + \frac{4V_{dc}}{\pi}\sum_{m=1}^{\infty}\sum_{n=-\infty}^{\infty}\left[\frac{1}{m}J_n(\frac{m\pi}{2}M)\sin((m+n)\frac{\pi}{2})\cos(m\omega_c t + n\omega_o t - \frac{2\pi}{5})\right] \quad (A.2)$$

$$v_{cn}(t) = V_{dc} + MV_{dc}\cos(\omega_o t - \frac{4\pi}{5}) + \frac{4V_{dc}}{\pi}\sum_{m=1}^{\infty}\sum_{n=-\infty}^{\infty}\left[\frac{1}{m}J_n(\frac{m\pi}{2}M)\sin((m+n)\frac{\pi}{2})\cos(m\omega_c t + n\omega_o t - \frac{4\pi}{5})\right] \quad (A.3)$$

$$v_{dn}(t) = V_{dc} + MV_{dc}\cos(\omega_o t - \frac{6\pi}{5}) + \frac{4V_{dc}}{\pi}\sum_{m=1}^{\infty}\sum_{n=-\infty}^{\infty}\left[\frac{1}{m}J_n(\frac{m\pi}{2}M)\sin((m+n)\frac{\pi}{2})\cos(m\omega_c t + n\omega_o t - \frac{6\pi}{5})\right] \quad (A.4)$$

$$v_{en}(t) = V_{dc} + MV_{dc}\cos(\omega_o t - \frac{8\pi}{5}) + \frac{4V_{dc}}{\pi}\sum_{m=1}^{\infty}\sum_{n=-\infty}^{\infty}\left[\frac{1}{m}J_n(\frac{m\pi}{2}M)\sin((m+n)\frac{\pi}{2})\cos(m\omega_c t + n\omega_o t - \frac{8\pi}{5})\right] \quad (A.5)$$

TABLE 1. Comparison of three-phase, five-phase, and seven-phase VSI.

	Load Structure	Maximum Line voltage	Harmonic loss $P_{h,cu} = R_e \cdot \left(\frac{V_{dc}}{L_\sigma}\right)^2 \frac{\Delta T^2}{48} f(M)$
			$f(M)$
Three-phase	Triangle	$v_{ab}(t) = \sqrt{3} M V_{dc} \cos(\omega_o t + \frac{\pi}{6}) + \frac{8V_{dc}}{\pi} \sum_{m=1}^{\infty} \sum_{n=-\infty}^{\infty} \left[\frac{1}{m} J_n(\frac{m\pi}{2} M) \sin((m+n)\frac{\pi}{2}) \sin(\frac{n\pi}{3}) \cos(m\omega_c t + n(\omega_o t - \frac{\pi}{3}) + \frac{\pi}{2}) \right]$	$f(M) = \frac{3}{2} M^2 - \frac{4\sqrt{3}}{\pi} M^3 + \frac{9}{8} M^4$
Five-phase	Pentagon	$v_{ac}(t) = 2 \sin\frac{2\pi}{5} M V_{dc} \cos(\omega_o t + \frac{\pi}{10}) + \frac{8V_{dc}}{\pi} \sum_{m=1}^{\infty} \sum_{n=-\infty}^{\infty} \left[\frac{1}{m} J_n(\frac{m\pi}{2} M) \sin((m+n)\frac{\pi}{2}) \sin(\frac{2n\pi}{5}) \cos(m\omega_c t + n(\omega_o t - \frac{2\pi}{5}) + \frac{\pi}{2}) \right]$	$f(M) = 2M^2 \sin^2\frac{2\pi}{5} - \frac{32}{3\pi} M^3 \sin^3\frac{2\pi}{5} + \frac{3}{2} M^4 \sin^2\frac{2\pi}{5}$
Seven-phase	Heptagon	$v_{ad}(t) = 2 \sin\frac{3\pi}{7} M V_{dc} \cos(\omega_o t + \frac{\pi}{14}) + \frac{8V_{dc}}{\pi} \sum_{m=1}^{\infty} \sum_{n=-\infty}^{\infty} \left[\frac{1}{m} J_n(\frac{m\pi}{2} M) \sin((m+n)\frac{\pi}{2}) \sin(\frac{3n\pi}{7}) \cos(m\omega_c t + n(\omega_o t - \frac{3\pi}{7}) + \frac{\pi}{2}) \right]$	$f(M) = 2M^2 \sin^2\frac{3\pi}{7} - \frac{32}{3\pi} M^3 \sin^3\frac{3\pi}{7} + \frac{3}{2} M^4 \sin^2\frac{3\pi}{7}$

TABLE 2. Comparison of errors in harmonic losses of five-phase VSI for $m_f = 9$.

M	DFI Analysis method	Analytical method	Absolute Error [%] of Analytical method	Simulation & FFT method	Absolute Error [%] of Simulation & FFT method
0.05	0.00397062	0.00428593	7.94107721	0.0063	58.0965696
0.1	0.0152092	0.015746	3.52944271	0.0182	12.9060867
0.15	0.0320178	0.0324405	1.32020314	0.0345	9.37249355
0.2	0.0524008	0.0526392	0.45495489	0.0565	6.13356989
0.25	0.0746785	0.0748213	0.1912197	0.081	4.63975269
0.3	0.0976354	0.0976753	0.04086633	0.1039	3.77462256
0.35	0.120303	0.120099	0.169571831	0.1284	3.54099642
0.4	0.141773	0.1412	0.404167225	0.1443	3.04690976
0.45	0.161276	0.160294	0.60889407	0.1659	3.57361544
0.5	0.178355	0.176909	0.81074262	0.1836	0.3526888
0.55	0.192869	0.190778	1.084155567	0.1994	1.71118904
0.6	0.204833	0.201847	1.457772917	0.2091	3.94441709
0.65	0.214349	0.210271	1.902504794	0.2209	1.23599952
0.7	0.221745	0.216411	2.405465738	0.2265	2.02993719
0.75	0.227676	0.220843	3.00119468	0.2313	2.5396508
0.8	0.233021	0.220843	5.226138417	0.241	4.01660846
0.85	0.238736	0.224347	6.027159708	0.2429	2.05379334
0.9	0.245926	0.227915	7.323747794	0.248	0.81558096
0.95	0.256074	0.240259	6.17594914	0.2636	4.22037673
1	0.270952	0.252064	6.970976409	0.268	0.43502236
			Average= 2.85231024		Average= 6.42199405

The following trigonometry formulas are considered:

$$\cos(\omega_o t) - \cos(\omega_o t - \frac{4\pi}{5}) = 2\sin(\frac{2\pi}{5})\cos(\omega_o t + \frac{\pi}{10}) \quad (A.6)$$

$$\cos(\omega_o t - \frac{2\pi}{5}) - \cos(\omega_o t - \frac{6\pi}{5}) = 2\sin(\frac{2\pi}{5})\cos(\omega_o t - \frac{3\pi}{10}) \quad (A.7)$$

$$\cos(\omega_o t - \frac{4\pi}{5}) - \cos(\omega_o t - \frac{8\pi}{5}) = 2\sin(\frac{2\pi}{5})\cos(\omega_o t - \frac{7\pi}{10}) \quad (A.8)$$

$$\cos(\omega_o t - \frac{6\pi}{5}) - \cos(\omega_o t) = 2\sin(\frac{2\pi}{5})\cos(\omega_o t - \frac{11\pi}{10}) \quad (A.9)$$

TABLE 3. Comparison of errors in harmonic losses of five-phase VSI for $m_f = 9$ and $m_f = 21$.

	m_f=9			m_f=21		
M	DFI Analysis method	Analytical method	Absolute Error [%] of Analytical method	DFI Analysis method	Analytical method	Absolute Error [%] of Analytical method
0.05	0.00397062	0.00428593	7.94107721	0.000728677	0.000787212	8.03305168
0.1	0.0152092	0.015746	3.52944271	0.0027907	0.00289212	3.63421364
0.15	0.0320178	0.0324405	1.32020314	0.0058732	0.00595845	1.45150855
0.2	0.0524008	0.0526392	0.45495489	0.009608	0.00966843	0.62895504
0.25	0.0746785	0.0748213	0.1912197	0.0136845	0.0137427	0.4252987
0.3	0.0976354	0.0976753	0.04086633	0.0178772	0.0179404	0.35352292
0.35	0.120303	0.120099	0.169571831	0.0220068	0.022059	0.23719941
0.4	0.141773	0.1412	0.404167225	0.0259057	0.0259347	0.11194448
0.45	0.161276	0.160294	0.60889407	0.0294313	0.0294418	0.0356763
0.5	0.178355	0.176909	0.81074262	0.0324959	0.0324934	0.00769328
0.55	0.192869	0.190778	1.084155567	0.0350675	0.0350409	0.07585371
0.6	0.204833	0.201847	1.457772917	0.0371424	0.037074	0.18415611
0.65	0.214349	0.210271	1.902504794	0.0387373	0.0386211	0.29996928
0.7	0.221745	0.216411	2.405465738	0.0399113	0.039749	0.40665175
0.75	0.227676	0.220843	3.00119468	0.0407818	0.0405629	0.53675904
0.8	0.233021	0.220843	5.226138417	0.0415036	0.0412065	0.71584152
0.85	0.238736	0.224347	6.027159708	0.042247	0.041862	0.91130731
0.9	0.245926	0.227915	7.323747794	0.0432166	0.0427498	1.0801405
0.95	0.256074	0.240259	6.17594914	0.0446869	0.0441292	1.24801676
1	0.270952	0.252064	6.970976409	0.046979	0.0462975	1.45064816
			Average= 2.85231024			Average= 1.09142041

TABLE 4. Comparison of overall time for calculating the harmonic loss in different methods.

Method	simulation	Writing a program	Number of calculations in the written program		Overall time needed
			Matlab function	Mathematical Operators	
Analytical analysis	No	Not necessary (a calculator is enough)	No	18	Very low
DFI analysis	No	Yes	Yes	(For time mf=9 & number of carrier harmonics=9) > 6693	medium
Applying the FFT to a simulated waveform	Yes	Yes	Yes	(For time window=0.2 sec & step time=2e-5) > 162500	high

$$\cos(\omega_o t - \frac{8\pi}{5}) - \cos(\omega_o t - \frac{2\pi}{5}) = 2\sin(\frac{2\pi}{5})\cos(\omega_o t - \frac{3\pi}{10}) \quad (A.10)$$

$$\cos(m\omega_c t + n\omega_o t) - \cos(m\omega_c t + n(\omega_o t - \frac{4\pi}{5})) = 2\sin(\frac{2n\pi}{5})\cos(m\omega_c t + n(\omega_o t - \frac{2\pi}{5}) + \frac{\pi}{2}) \quad (A.11)$$

$$\cos(m\omega_c t + n(\omega_o t - \frac{2\pi}{5})) - \cos(m\omega_c t + n(\omega_o t - \frac{6\pi}{5})) = 2\sin(\frac{2n\pi}{5})\cos(m\omega_c t + n(\omega_o t - \frac{4\pi}{5}) + \frac{\pi}{2}) \quad (A.12)$$

$$\cos(m\omega_c t + n(\omega_o t - \frac{4\pi}{5})) - \cos(m\omega_c t + n(\omega_o t - \frac{8\pi}{5})) = 2\sin(\frac{2n\pi}{5})\cos(m\omega_c t + n(\omega_o t - \frac{6\pi}{5}) + \frac{\pi}{2}) \quad (A.13)$$

$$\cos(m\omega_c t + n(\omega_o t - \frac{6\pi}{5})) - \cos(m\omega_c t + n(\omega_o t)) = 2\sin(\frac{2n\pi}{5})\cos(m\omega_c t + n(\omega_o t - \frac{3\pi}{5}) - \frac{\pi}{2}) \quad (A.14)$$

$$\cos(m\omega_c t + n(\omega_o t - \frac{8\pi}{5})) - \cos(m\omega_c t + n(\omega_o t - \frac{2\pi}{5})) = 2\sin(\frac{2n\pi}{5})\cos(m\omega_c t + n(\omega_o t - \pi) - \frac{\pi}{2}) \quad (A.15)$$

Note that the trigonometry formulas (A.6)-(A.15) are extracted using the following trigonometric relation:

$$\cos(\alpha) - \cos(\beta) = -2\sin(\frac{\alpha+\beta}{2})\sin(\frac{\alpha-\beta}{2}) \quad (A.16)$$

Using the vector diagram, the line-to-line voltage v_{ac} can be expressed as:

$$v_{ac}(t) = v_{an}(t) - v_{cn}(t) \quad (A.17)$$

Therefore, substituting (A.1) and (A.3) into (A.17) and after applying (A.6), (A.11) and simplifying, the line-to-line voltage v_{ac} can be calculated as:

$$v_{ac}(t) = 2\sin\frac{2\pi}{5}MV_{dc}\cos(\omega_o t+\frac{\pi}{10}) + \frac{8V_{dc}}{\pi}\sum_{m=1}^{\infty}\sum_{n=-\infty}^{\infty}\left[\begin{array}{l}\frac{1}{m}J_n(\frac{m\pi}{2}M)\sin((m+n)\frac{\pi}{2})\\ \sin(\frac{2n\pi}{5})\cos(m\omega_c t\\ \quad + n(\omega_o t-\frac{2\pi}{5})+\frac{\pi}{2})\end{array}\right] \tag{A.18}$$

The other line-to-line voltages can be calculated in the same way:

$$v_{bd}(t) = 2\sin\frac{2\pi}{5}MV_{dc}\cos(\omega_o t-\frac{3\pi}{10}) + \frac{8V_{dc}}{\pi}\sum_{m=1}^{\infty}\sum_{n=-\infty}^{\infty}\left[\begin{array}{l}\frac{1}{m}J_n(\frac{m\pi}{2}M)\sin((m+n)\frac{\pi}{2})\\ \sin(\frac{2n\pi}{5})\cos(m\omega_c t\\ \quad + n(\omega_o t-\frac{4\pi}{5})+\frac{\pi}{2})\end{array}\right] \tag{A.19}$$

$$v_{ce}(t) = 2\sin\frac{2\pi}{5}MV_{dc}\cos(\omega_o t-\frac{7\pi}{10}) + \frac{8V_{dc}}{\pi}\sum_{m=1}^{\infty}\sum_{n=-\infty}^{\infty}\left[\begin{array}{l}\frac{1}{m}J_n(\frac{m\pi}{2}M)\sin((m+n)\frac{\pi}{2})\\ \sin(\frac{2n\pi}{5})\cos(m\omega_c t\\ \quad + n(\omega_o t-\frac{6\pi}{5})+\frac{\pi}{2})\end{array}\right] \tag{A.20}$$

$$v_{da}(t) = 2\sin\frac{2\pi}{5}MV_{dc}\cos(\omega_o t-\frac{11\pi}{10}) + \frac{8V_{dc}}{\pi}\sum_{m=1}^{\infty}\sum_{n=-\infty}^{\infty}\left[\begin{array}{l}\frac{1}{m}J_n(\frac{m\pi}{2}M)\sin((m+n)\frac{\pi}{2})\\ \sin(\frac{3n\pi}{5})\cos(m\omega_c t\\ \quad + n(\omega_o t-\frac{3\pi}{5})+\frac{\pi}{2})\end{array}\right] \tag{A.21}$$

$$v_{eb}(t) = 2\sin\frac{2\pi}{5}MV_{dc}\cos(\omega_o t-\frac{3\pi}{2}) + \frac{8V_{dc}}{\pi}\sum_{m=1}^{\infty}\sum_{n=-\infty}^{\infty}\left[\begin{array}{l}\frac{1}{m}J_n(\frac{m\pi}{2}M)\sin((m+n)\frac{\pi}{2})\\ \sin(\frac{3n\pi}{5})\cos(m\omega_c t\\ \quad + n(\omega_o t-\pi)-\frac{\pi}{2})\end{array}\right] \tag{A.22}$$

REFERENCES

[1] L. Gao and J. E. Fletcher, "A space vector switching strategy for three-level five-phase inverter drives," *IEEE Trans. Ind. Electron.*, vol. 57, no. 7, pp. 2332–2343, Jul. 2010, doi: 10.1109/TIE.2009.2033087.

[2] B. S. Umesh and K. Sivakumar, "Multilevel inverter scheme for performance improvement of pole-phase-modulated multiphase induction motor drive," *IEEE Trans. Ind. Electron.*, vol. 63, no. 4, pp. 2036–2043, Apr. 2016, doi: 10.1109/TIE.2015.2506623.

[3] H. Pairo, M. H. Khanzade, and A. Shoulaie, "Maximum efficiency control of six- and three-phase two-motor drives," *J. Eng.*, vol. 2017, no. 7, pp. 410–417, Jul. 2017, doi: 10.1049/joe.2017.0262.

[4] D. Glose and R. Kennel, "Continuous space vector modulation for symmetrical six-phase drives," *IEEE Trans. Power Electron.*, vol. 31, no. 5, pp. 3837–3848, May 2016, doi: 10.1109/TPEL.2015.2456234.

[5] D. Glose and R. Kennel, "Carrier-based pulse width modulation for symmetrical six-phase drives," *IEEE Trans. Power Electron.*, vol. 30, no. 12, pp. 6873–6882, Dec. 2015, doi: 10.1109/TPEL.2015.2389896.

[6] J. Prieto, M. Jones, F. Barrero, E. Levi, and S. Toral, "Comparative analysis of discontinuous and continuous PWM techniques in VSI-fed five-phase induction motor," *IEEE Trans. Ind. Electron.*, vol. 58, no. 12, pp. 5324–5335, Dec. 2011, doi: 10.1109/TIE.2011.2126540.

[7] G. K. Singh, K. Nam, and S. K. Lim, "A simple indirect field-oriented control scheme for multiphase induction machine," *IEEE Trans. Ind. Electron.*, vol. 52, no. 4, pp. 1177–1184, Aug. 2005, doi: 10.1109/TIE.2005.851593.

[8] D. Dujic, M. Jones, and E. Levi, "Analysis of output current-ripple RMS in multiphase drives using polygon approach," *IEEE Trans. Power Electron.*, vol. 25, no. 7, pp. 1838–1849, Jul. 2010, doi: 10.1109/TPEL.2010.2042969.

[9] M. Jones, S. N. Vukosavic, D. Dujic, and E. Levi, "A synchronous current control scheme for multiphase induction motor drives," *IEEE Trans. Energy Convers.*, vol. 24, no. 4, pp. 860–868, Dec. 2009, doi: 10.1109/TEC.2009.2025419.

[10] E. Levi, R. Bojoi, F. Profumo, H. Toliyat, and S. Williamson, "Multi-phase induction motor drives—A technology status review," *IET Electr. Power Appl.*, vol. 1, no. 4, pp. 489–516, Jul. 2007, doi: 10.1049/iet-epa:20060342.

[11] E. Levi, "Multiphase electric machines for variable-speed applications," *IEEE Trans. Ind. Electron.*, vol. 55, no. 5, pp. 1893–1909, May 2008, doi: 10.1109/TIE.2008.918488.

[12] E. Levi, S. N. Vukosavic, and M. Jones, "Vector control schemes for series-connected six-phase two-motor drive systems," *IEE Proc.-Electr. Power Appl.*, vol. 152, no. 2, pp. 226–238, Mar. 2005, doi: 10.1049/ip-epa:20055018.

[13] E. Levi, M. Jones, S. N. Vukosavic, and H. A. Toliyat, "Operating principles of a novel multiphase multimotor vector-controlled drive," *IEEE Trans. Energy Convers.*, vol. 19, no. 3, pp. 508–517, Sep. 2004, doi: 10.1109/TEC.2004.832055.

[14] E. Levi, M. Jones, S. N. Vukosavic, and H. A. Toliyat, "A novel concept of a multiphase, multimotor vector controlled drive system supplied from a single voltage source inverter," *IEEE Trans. Power Electron.*, vol. 19, no. 2, pp. 320–335, Mar. 2004, doi: 10.1109/TPEL.2003.823241.

[15] S. Williamson and S. Smith, "Pulsating torque and losses in multiphase induction machines," *IEEE Trans. Ind. Appl.*, vol. 39, no. 4, pp. 986–993, Jul./Aug. 2003, doi: 10.1109/TIA.2003.813722.

[16] E. E. Ward and H. Harer, "Preliminary investigation of an inverter-fed 5-phase induction motor," *Proc. IEE*, vol. 116, no. 6, pp. 980–984, 1969, doi: 10.1049/piee.1969.0182.

[17] F. Acosta-Cambranis, J. Zaragoza, L. Romeral, and N. Berbel, "Comparative analysis of SVM techniques for a five-phase VSI based on SiC devices," *Energies*, vol. 13, no. 24, p. 6581, Dec. 2020, doi: 10.3390/en13246581.

[18] J.-S. Hu, K.-Y. Chen, T.-Y. Shen, and C.-H. Tang, "Analytical solutions of multilevel space-vector PWM for multiphase voltage source inverters," *IEEE Trans. Power Electron.*, vol. 26, no. 5, pp. 1489–1502, May 2011, doi: 10.1109/TPEL.2010.2084107.

[19] Ó. López, J. Álvarez, J. Doval-Gandoy, and F. D. Freijedo, "Multilevel multiphase space vector PWM algorithm," *IEEE Trans. Ind. Electron.*, vol. 55, no. 5, pp. 1933–1942, May 2008, doi: 10.1109/TIE.2008.918466.

[20] M. Jones, D. Dujic, E. Levi, J. Prieto, and F. Barrero, "Switching ripple characteristics of space vector PWM schemes for five-phase two-level voltage source inverters—Part 2: Current ripple," *IEEE Trans. Ind. Electron.*, vol. 58, no. 7, pp. 2799–2808, Jul. 2011, doi: 10.1109/TIE.2010.2070778.

[21] S. Halász, "Continuous PWM strategies of multi-phase inverter-fed AC drives," *Periodica Polytechnica Electr. Eng. Comput. Sci.*, vol. 56, no. 2, pp. 51–62, 2012, doi: 10.3311/PPee.7161.

[22] B. Wu, *High-Power Converters and AC Drives*. Hoboken, NJ, USA: Wiley, 2006, pp. 119–141.
[23] M. H. J. Bollen, *Understanding Power Quality Problems: Voltage Sags and Interruptions*. Hoboken, NJ, USA: Wiley, 1999.
[24] W. Rui, S. Qiuye, M. Dazhong, and H. Xuguang, "Line impedance cooperative stability region identification method for grid-tied inverters under weak grids," *IEEE Trans. Smart Grid*, vol. 11, no. 4, pp. 2856–2866, Jul. 2020, doi: 10.1109/TSG.2020.2970174.
[25] D. G. Holmes and T. A. Lipo, *Pulse Width Modulation for Power Converters: Principles and Practice*. Hoboken, NJ, USA: Wiley, 2003.
[26] D. Dujic, E. Levi, and M. Jones, "Harmonic losses of multiphase PWM inverter-fed drives," in *Proc. IEEE Energy Convers. Congr. Expo.*, San Jose, CA, USA, Sep. 2009, pp. 861–868, doi: 10.1109/ECCE.2009.5316575.
[27] P. Hamedani, "Harmonic evaluation of seven-phase VSI with PWM switching teqnique," in *Proc. 11th Power Electron., Drive Syst., Technol. Conf. (PEDSTC)*, Tehran, Iran, Feb. 2020, pp. 1–6, doi: 10.1109/PEDSTC49159.2020.9088377.

PEGAH HAMEDANI received the B.Sc. and M.Sc. degrees from the University of Isfahan, Isfahan, Iran, in 2007 and 2009, respectively, and the Ph.D. degree from the Iran University of Science and Technology, Tehran, in 2016, all in electrical engineering. She is currently an Assistant Professor with the Department of Railway Engineering and Transportation Planning, University of Isfahan. Her research interests include power electronics, control of electrical motor drives, supply system of the electric railway (AC and DC), linear motors & MAGLEVs, and analysis of overhead contact systems. She was a recipient of the IEEE 11th Power Electronics, Drive Systems, and Technologies Conference (PEDSTC'20) Best Paper Award, in 2020.

CRISTIAN GARCIA (Member, IEEE) received the M.Sc. and Ph.D. degrees in electronics engineering from Universidad Tecnica Federico Santa Maria, Valparaiso, Chile, in 2013 and 2017, respectively.

From 2017 to 2019, he was with the Engineering Faculty, Universidad Andres Bello, Santiago, Chile, as an Assistant Professor. Since 2019, he has been with the Department of Electrical Engineering, University of Talca, Curico, Chile, where he is currently an Assistant Professor. In 2016, he was a Visiting Ph.D. Student with the Power Electronics Machines and Control (PEMC) Group, University of Nottingham, U.K. His research interests include electric transportation applications, variable-speed drives, and model predictive control of power converters and drives.

JOSE RODRIGUEZ (Life Fellow, IEEE) received the Engineering degree in electrical engineering from Universidad Tecnica Federico Santa Maria, Valparaiso, Chile, in 1977, and the Dr.-Ing. degree in electrical engineering from the University of Erlangen, Erlangen, Germany, in 1985. He has been with the Department of Electronics Engineering, Universidad Tecnica Federico Santa Maria, since 1977, where he was a Full Professor and the President. Since 2015, he has been the President and since 2019, he has been a Full Professor with Universidad Andres Bello, Santiago, Chile. He has coauthored two books, several book chapters and more than 400 journals and conference papers. His research interests include multilevel inverters, new converter topologies, control of power converters, and adjustable-speed drives. He has received a number of best paper awards from journals of the IEEE. He is a member of the Chilean Academy of Engineering. In 2014, he received the National Award of Applied Sciences and Technology from the Government of Chile. In 2015, he received the Eugene Mittelmann Award from the Industrial Electronics Society of the IEEE. From 2014 to 2020, he was included in the list of Highly Cited Researchers published by Web of Science.